April 2002

Aerosol optical depth at Cape Grim, Tasmania 1986-1999

Stephen R. Wilson
University of Wollongong, swilson@uow.edu.au

B. W. Forgan
Australian Bureau of Meteorology

Aerosol optical depth at Cape Grim, Tasmania 1986-1999

Abstract

The aerosol optical depth at 4 wavelengths (368, 500, 778 and 868nm) has been measured automatically at Cape Grim since 1986. The site, on the northwest tip of Tasmania, Australia was chosen to be representative of much of the southern ocean. Fourteen years of measurement have been calibrated and analyzed. The data have been filtered so that only measurements made under on-shore wind conditions are considered. The major feature observed in the record is the eruption of Mt Pinatubo, which resulted in the aerosol optical depth at 500 nm rising to 0.2 – 0.3. If the period of high stratospheric aerosol is ignored, the resulting record shows an average aerosol optical depth near 0.04 for all four wavelengths. In the winter months the observed optical depth correlates well with wind speed. This correlation indicates, that, as an annual average, 40% of the observed aerosol optical depth is due to wind-generated aerosol. The annual cycle of the aerosol optical depth can be understood in terms of the impact of photochemically generated aerosol in the summer months, and an injection of mid-tropospheric aerosol in September, presumably due to biomass burning.

Keywords

aerosol, optical depth, Sun photometer, Southern Hemisphere, GeoQUEST

Disciplines

Life Sciences | Physical Sciences and Mathematics | Social and Behavioral Sciences

Publication Details

This article was originally published as Wilson, SR and Forgan, BW, Aerosol optical depth at Cape Grim, Tasmania 1986-1999, Journal of Geophysical Research, 107(D8), 10.1029/2001JD000398, 2002.

Aerosol optical depth at Cape Grim, Tasmania 1986-1999

S.R. Wilson and B.W. Forgan*

Dept. of Chemistry, University of Wollongong, Wollongong, 2522, NSW, Australia

*Observations and Engineering Branch, Bureau of Meteorology, GPO Box 1289K, Melbourne, Vic., 3001, Australia

Abstract

The aerosol optical depth at 4 wavelengths (368, 500, 778 and 868nm) has been measured automatically at Cape Grim since 1986. The site, on the northwest tip of Tasmania, Australia was chosen to be representative of much of the southern ocean. Fourteen years of measurement have been calibrated and analyzed. The data have been filtered so that only measurements made under on-shore wind conditions are considered. The major feature observed in the record is the eruption of Mt Pinatubo, which resulted in the aerosol optical depth at 500 nm rising to 0.2 – 0.3. If the period of high stratospheric aerosol is ignored, the resulting record shows an average aerosol optical depth near 0.04 for all four wavelengths. In the winter months the observed optical depth correlates well with wind speed. This correlation indicates, that, as an annual average, 40% of the observed aerosol optical depth is due to wind-generated aerosol. The annual cycle of the aerosol optical depth can be understood in terms of the impact of photochemically generated aerosol in the summer months, and an injection of mid-tropospheric aerosol in September, presumably due to biomass burning.

Introduction

A Baseline Air Pollution Station was established at Cape Grim (40°40'56", 144°41'18"E) to study the chemistry of the atmosphere where the composition is dominated by the southern oceans. Knowledge of the physical and optical properties of the aerosol is fundamental to understanding chemical processes. One of the prime measurements of aerosol optical activity is the aerosol optical depth, which can be measured by looking at the direct solar irradiance. However, the climate at Cape Grim is both cloudy and windy, making clear sun solar irradiance measurements difficult. The cloudiness limits the available measurement time, the wind stresses mechanical systems required to point detectors at the sun and the marine environment makes it difficult to maintain equipment due to corrosion and the build up of salt films on optical surfaces. Besides equipment failures, this leads to significant uncertainty in any results.

Direct (beam) solar spectral irradiance measurements at Cape Grim have been reported previously, involving the use of hand-held photometers (Volz) over the period 1978 to 1984 [*Ethridge et al.*, 1984; *Platt and Patterson*, 1986]. Following these measurements, significant alterations were made to the spectral irradiance program to permit reliable and systematic transmission measurements. These changes were to permit the determination of aerosol optical depth (δ_a) with an uncertainty much less that the (small) aerosol optical depths observed at Cape Grim.

As δ_a is a vertically integrated (column) measurement, the results can be influenced by aerosol at distinctly different altitudes above the site. The three main categories relevant to Cape Grim are injections of volcanic aerosol into the stratosphere, free troposphere aerosol either transported large distances from their source or generated through cloud action [*Clarke et al.*, 1998]; and also the marine boundary layer aerosol from either sea-salt or from gas-to-particle conversion.

This paper presents an overview of the Cape Grim δ_a record, as measured at 4 wavelengths (368nm, 500nm, 778nm and 868nm), for the period 1985 – 1997. It highlights the impact of volcanic eruptions on the δ_a record, documents the impact of wind on δ_a, and analyses the δ_a annual cycle to identify possible aerosol sources.

Measurement program

Aerosol optical depth is the measure of extinction by aerosols (or suspended particular matter) in the vertical atmospheric, and is a quantity derived from values of transmission in spectral bands where the primary components of extinction are molecular (δ_m), aerosol (δ_a) and ozone extinction (δ_o). Deriving δ_a is in principle a simple exercise using the Lambert-Beer-Bouguer law as applied to direct sun observations in the atmosphere, namely:

$$\ln S(t,\lambda,m) = \ln S_0(\lambda) - 2\ln(r(t)/r_0) - \delta_m m_m - \delta_a m_a - \delta_o m_o \qquad (1)$$

where $S(t, \lambda, m)$ is the signal from the sun monitoring radiometer at time t, wavelength λ and representative relative air mass m, and $S_o(\lambda)$ is the sun signal at the top of the atmosphere when the earth is at distance of 1 AU (r_o) from the sun. The relative air mass [*Forgan*, 1988] for the molecular (m_m), ozone (m_o) and aerosol (m_a) are dependent on the direct irradiance path through the atmosphere. In principle knowledge of the time and location of an observation, together with the atmospheric pressure, allows these terms to be estimated. An appropriate choice of wavelength allows the impact of ozone to be minimized (small δ_o) and hence δ_a determined.

While the principle of the measurement is simple, the instability of the equipment used to measure the optical transmission and the relatively low magnitude of δ_a at Cape Grim, means that assigning a useful value for $S_o(\lambda)$, required considerable effort.

Instrumentation

Between 1986 and December 1997 the direct solar spectral irradiance signals $S(t, \lambda, m)$ were measured with a radiometer based on the design proposed by the World Radiation Centre, Davos [*WMO*, 1979]. The instrument, designated WMO#1, consisted of four independent spectral radiometers with full fields of view of 2.4° and slope angle 0.8° and mounted in a single weatherproof housing. Each radiometer used a filter-detector combination in a temperature-stabilized housing maintained at 40 °C. The filters were 25 mm diameter interference filters with full width at half maximum of 5 nm, with peak transmission at approximately 368, 500, 778 and 868 nm. From December 1997, WMO#1 was replaced with a Carter-Scott Design SPO1A radiometer based on similar principles to the WMO#1 but temperature-stabilized at 30°C; the data from the SPO1A will be reported in detail in another paper.

The WMO#1 was mounted onto 3 different trackers over its period of operation at Cape Grim. The initial tracking system was a passive polar–axis clock-drive which required manual adjustment for the change in solar declination. The high wind conditions (annual average 40 km/hr) and staffing arrangements at the site meant that tracking failures were frequent. In 1987 the system was replaced with an active polar-axis tracking system that actively adjusted the clock-derived position using a filtered quadrant detector [*Sibson and Forgan*, 1987]. This system kept the WMO#1 aligned to within 0.05° of the solar position and failure rates decreased significantly. In 1995 this polar–axis system was replaced with a rugged altitude-azimuth tracker with active adjustment to within 0.025° of the sun.

The stability of the 368 nm filter-detector proved problematic for the entire period of WMO#1 operation analyzed here. The 368 nm interference filter had to be replaced twice because the transmission of each filter had decayed markedly. The first change occurred in mid-1986 and the latter in 1994. The degradation was traced to poor filter

manufacture, the continuous exposure of the filters to solar energy and maintaining of the filters at a temperature of 40°C. Degradation of the 500, 778 and 868 nm filters was not rapid and the same filters were used from 1986 until measurements with WMO#1 ceased. The filter-detector spectral radiometers of the SPO1A type deployed in Australian network operations post-1995 have proven much more stable, through judicious choice of the filter manufacturing process and filter diameter, shuttering to reduce solar exposure, and temperature stabilization at 30°C.

The high wind and salt laden climate meant that frequent cleaning of the front glass windows of the radiometers was required. Staffing of the site meant that on some occasions data had to be flagged and later eliminated because of dirty front glass windows. Periods eliminated for this reason were typically early mornings prior to staff arriving at the site.

Data collection

The voltage signals from WMO#1 peaked in the range of 1 to 5 V during clear sun conditions, and were monitored by an auto-ranging integrating digital voltmeter with a signal resolution of 1 μV. The digital voltmeter integrated the voltage signals over 2 power line cycles (at 50 Hz) to reduce noise. Examination of the zero irradiance signals at night (after astronomical twilight) indicates that the precision of the reported WMO#1 irradiance signals was better than 5 μV.

A voltage measurement from each detector was taken every 6 seconds during a minute, starting at 3 seconds past the start of the minute. From these 10 measurements, the average for the minute, the maximum and minimum signal during the minute, the unbiased estimate of the standard deviation, and the first measurement of the minute were stored. These data were recorded with similar measurements of atmospheric pressure, temperature, wind speed and direction for every minute of the day [*Walford*, 1987]. The

time was recorded in Australian Eastern Standard Time and maintained to within ±3 seconds of the true time.

Calibration

Calibration of WMO#1 (that is, determination of an appropriate *ln* $S_o(\lambda)$ for each day of the record) was via a two step process. Firstly, the calibration of the 868 nm filter-detector was determined, and then used as the reference in applying the general method [*Forgan*, 1994] to obtain the calibration of the other 3 channels.

The calibration of the 868 nm sensor was achieved by first reducing each day's observations (using the first measurement in each minute) to leave only clear sun observations by a series of objective filters (to be presented elsewhere). These filtered measurements were then divided into morning and afternoon periods. From each of these periods data were selected for the time between $m_a = 6$ and the next 90 minutes closer to solar noon. Provided that more than 30 valid measurements remained in the period, least squares regression (LSR) analyses were performed using modified forms of equation (1) as the regression model, namely:

$$\left(\ln S(t,\lambda,m) + 2\ln(r(t)/r_0) + \delta_m m_m\right) = \left\langle \ln S_0(\lambda)\right\rangle_1 - \left\langle \delta_a \right\rangle_1 m_a \qquad (2)$$

and

$$\left(\ln S(t,\lambda,m) + 2\ln(r(t)/r_0) + \delta_m m_m\right)/m_a = -\left\langle \delta_a \right\rangle_2 + \left\langle \ln S_0(\lambda)\right\rangle_2 / m_a \qquad (3)$$

Both are solved for $\langle \ln S_o(\lambda)\rangle_i$ and $\langle \delta_a \rangle_i$. Equation (2) is a common modified form of the Bouguer-Lambert-Beer law and equation (3) is an adaptation of a commonly used technique in astronomy [*Young*, 1974]. Both these applications of the LSR minimize the impact of poor representative air mass selection [*Forgan*, 1994] by removing the influence of $\delta_m m_m$.

The mean of the two estimates of $\langle \ln S_o(868\text{ nm})\rangle$, that is

$$\left\langle \ln S_0(868nm) \right\rangle = 0.5(\left\langle \ln S_0(868nm) \right\rangle_1 + \left\langle \ln S_0(868nm) \right\rangle_2), \quad (4)$$

was obtained. If the standard error of the LSR analysis for equation (2) was less than 0.001, then the intra-diurnal period value is accepted for further analysis.

This process produces numerous estimates of the calibration at 868 nm. The final calibration value for 868 nm for any day was based on a polynomial LSR of all these accepted values over the sequence of days (and years) bounded by significant changes in calibration, normally due to instrument alterations. The polynomial LSR was preferred to monthly or running means because of the paucity of accepted values.

Given the 868 nm calibration derived from the polynomial fit, the general method [Equation 9, *Forgan*, 1994] is applied for the remaining wavelengths to the same time set of data used to generate the 868 nm calibrations. Once again polynomial LSR analyses of the accepted periods are used to give the final values for $\left\langle \ln S_0(\lambda) \right\rangle$.

In using the general method, estimates of ozone extinction are required for the analysis of the 500 nm filter-detector; in this case the annual mean ozone column amount for Melbourne, Australia was used [*Atkinson and Easson*, 1989]. Other ozone estimates could be used (such as satellite measurements), but the sensitivity of the retrieval to the ozone assumption is small. If the column ozone amount was wrong by 30%, this would result in an error in $\left\langle \ln S_0(\lambda) \right\rangle$ of less than 0.0003.

The calibration factors for two of the sensors are shown in Figure 1. It can be seen that the calibration value of each sensor decreases over the period of the measurements, with a step change as the new sunphotometer (SPO1A) was introduced in December 1997. Beyond this general trend there is evidence of small-scale structure in the values, particularly for the 500 nm sensor during 1990. The presence of such structures poses a fundamental problem in the analysis of the radiometer. While such variation can be fitted by a polynomial, there is no *a priori* reason to favor particular time dependences given

there is no independent verification of the instrument stability or the suitability of monthly mean ozone data in the general method, and hence there is a real possibility that the chosen form will introduce an error of unknown magnitude through certain parts of the record. Furthermore, the models used to determine the various air mass and extinction components, and the values used for the sensor characteristics such as wavelength lead to further sources of uncertainty.

A detailed uncertainty analysis [*ISO*, 1995] was performed on the measurement system and the subsequent derivation of aerosol optical depth for any time (*t)*. The analysis suggests that using a consistent model for molecular and ozone extinction, and a calibration value estimated from at least 30 equivalent samples, the U_{95} (95% confidence interval) in aerosol optical depth for all four wavelengths is less than 0.010.

Derivation of aerosol optical depth

Calibration of the each sensor provides one method of determining δ_a for each individual clear sun observation (190,000 in total for the period investigated here) using eqn. (1), and then averaging the derived δ_a over an appropriate interval. This has been performed for each morning and afternoon period with more than 30 clear sun measurements between $m_a = 6$ and solar noon, resulting in a mean estimate $\overline{\delta}_a$.

One means of avoiding a calibration bias as outlined above is to use the $\langle \delta_a \rangle$ derived from equations (2) and (3), as they are derived without the assumption of $\langle \ln S_0(\lambda) \rangle$. A comparison of the results from equations (2) and (3) indicates that 95% of the differences are less than 0.001. However, these data are biased to clear sky periods in early morning or late afternoon and have not been used in the analyses presented below.

Results and Discussion

Overview

Using the half-day averages there are over 2300 estimates of $\overline{\delta}_a$ for the period 1986 – June 1997, prior to any other data selection. For the same period there are 1560 estimates of $\langle \delta_a \rangle$.

To remove the impact of local or regional pollution sources, the measurements have been separated based on the wind direction (10m vector hourly average [*Walford*, 1987]) prevailing during the middle of the optical depth measurement. If the calculated direction lies within the Cape Grim "baseline" or clean-air sector (190-280 deg) it has been included in the baseline data set (1200 $\overline{\delta}_a$ and 730 $\langle \delta_a \rangle$ values remain). As a test of the impact of a more rigorous filtering procedure, the data has also been selected using the CO_2 baseline criterion [*Beardsmore and Pearman*, 1987; *Dick et al.*, 1996]. This leaves only 875 valid $\overline{\delta}_a$ "baseline" values. No significant difference at the 95% confidence interval has been observed in the resulting averages determined using the two definitions of "baseline" used, and so the wind-based definition dataset is used.

The $\overline{\delta}_a$ data have been summarized into medians. Figure 2 shows the monthly medians of entire data set, while Figure 3 shows the results using the baseline-selected data, using a 90-day running median to compensate for the reduction in data. The dominant feature is the rapid rise in δ_a in July 1991 due to the explosion of Mt. Pinatubo. This rise is similar in timing and magnitude to reported observations in Antarctica [*Herber et al.*, 1996]. The impact of the volcanic aerosol decays away slowly following the injection into the stratosphere, and δ_a values return close to normal values by the end of the data record.

The two optical depth records show a preference for δ_a to be less during baseline periods than at other times. For baseline periods free from volcanic perturbation δ_a at all wavelengths is typically less that 0.05. This is significantly less than observed in earlier

measurements that reported values closer to 0.1 at 500 nm [*Platt and Patterson*, 1986]. It has been shown that the earlier measurements are subject to large uncertainties [*Forgan*, 1987], given the frequency of calibration, deteriorating filters and operator preference for measurement conditions, that is typical with measurements from hand held instruments in harsh environments [*WMO*, 1994]. These factors presumably led to the higher δ_a reported by Platt and Patterson [1986].

In order to understand the primary factors affecting δ_a during 1986-1997, the impact of stratospheric aerosol will be examined, followed by a study of the annual cycle. Finally, variations attributable to local conditions will be examined.

Impact of volcanic aerosol

The eruption of Mt. Pinatubo had a major impact on global aerosol levels [E.g. *Russell et al.*, 1996], and as already noted is clearly evident in the Cape Grim δ_a record. In order to evaluate the impact of stratospheric aerosol on this record, the monthly average stratospheric aerosol measurements of SAGE II [*Thomason*, 1998] have been used for the 5º-latitude band centered on 42.5º S. The SAGE II wavelengths do not match those of WMO#1, so aerosol optical depths estimates (δ_S) for Cape Grim have been estimated via a logarithmic interpolation for the 3 longer wavelengths, and for 368 nm the aerosol optical depth has been assumed to be the same as that measured at 385nm. This stratospheric aerosol component δ_S can be subtracted from δ_a to leave the tropospheric component. The result of this process for 868nm is shown in Figure 4a. This shows that this process is largely successful, although the period from July 1991 through to June 1992 remains significantly perturbed. This is more easily seen in Figure 4b, where the seasonal cycle (discussed below) has been removed as well. A second period of raised δ_a is also apparent in February and March 1997, although the cause here is unknown. It is a part of the data record with relatively few measurements (12 for the March median), and

so a few measurements with high optical depth can have a significant impact. Also, there were large bush-fires recorded south of the station during part of this time (S. Baly, 2000, personal communication).

It appears that the volcanic component of δ_a at Cape Grim was higher than the estimated SAGE II values for the last part of 1991, presumably due to spatial inhomogeneity in the stratospheric aerosol distribution during the initial phase of the plume dispersal. After this period, the δ_S data appear to capture the loss of stratospheric aerosol well, with the calculated "tropospheric" aerosol showing little perturbation.

Analysis of the Cape Grim δ_a record after December 1992 shows that the signal decays away with a lifetime of approximately 19±2 months at 868nm. This is longer than the estimates from the Arctic of 11±4 months [*Beyerle et al.*, 1995] and 14 months [*Nagel et al.*, 1998], although it is not clear whether the difference is significant.

The annual cycle

From Figure 3 it can be seen that there is evidence of an annual cycle in the baseline-selected δ_a. To quantify the annual cycle, the period significantly perturbed by the Mt. Pinatubo aerosol (7/1991 – 6/1992) has been removed and all remaining measurements have then had the stratospheric signal removed, as outlined above. The median of the values for each month is shown in Figure 5(a) and in Table 1, which was determined using $\overline{\delta}_a$. This shows a minimum in aerosol optical depth in winter (June – July), followed by a rapid rise in August, with a maximum in September. The optical depth then decreases until summer, where it plateaus until April, when it then decays away to the winter values. The increased scatter in the middle of the year is partially due to the lack of clear-sun measurements for LSR analysis during this (winter) period.

For the purposes of removing the annual cycle from the record, as shown in figure 4b, the difference between the annual average and the monthly means (see Table 1) has been

calculated. This difference has then been used as the estimate of the annual cycle, and removed from the data.

Impact of wind on observed AOD

As there is an annual variation in wind speed (Figure 5(b)), part of the cycle may be due to wind-generated sea salt, and this will now be investigated. It has been known for a long time that sea-salt concentrations depend on wind speed within the marine boundary layer [*Woodcock*, 1953]. A number of studies have looked at this dependence and Gong *et al.* [1997] present a summary of the results, along with their model results. They report a near linear relationship between log(mass of aerosol) and wind speed. (Note that both decadic (log) and natural (ln) logarithms values are reported in literature. For this wind study decadic logarithms have been used).

To investigate the impact of wind speed could be seen in the Cape Grim δ_a record, the baseline data from June and July has been studied, excluding the 12 months after the Mt. Pinatubo eruption. As before, the stratospheric aerosol component has been removed. The period June - July has been chosen so as to maximize the impact of boundary-layer sea-salt scattering, as Gras and Ayers [1983] have shown that in this seasonal period the surface level aerosol is dominated by sea salt. These data were sorted, based on the mid-measurement hourly vector wind speed [*Walford*, 1987]. The lifetime of the particles generated is expected to be of the order of 2 days [*Gong et al.*, 1997], so the hourly average wind speed is only a rough proxy for the air mass environment for the 2 days prior to arrival at Cape Grim. The resultant data set was sorted into bins based on the wind speed. Each bin was ±1 m/s wide, and spaced in 2 m/s wind speed increments. The median of each bin was then calculated. Due to the extensive selection process, only 92 half days of $\overline{\delta}_a$ were available.

The result of this is shown in Figure 6 for all four wavelengths. There is no consistent pattern between the wavelengths, as is expected for (near neutral) extinction by large aerosol at the wavelengths used. It can be seen that $\overline{\delta_a}$ at the lowest wind speeds (<2m s^{-1}) is higher than those at stronger winds (< 10m s^{-1}). This is consistent with observations of particle numbers (J. Gras, personal communication, 1999), and is presumably caused by local particle generation. At higher wind speeds there is a clear dependence of δ_a on wind speed. Condensation Nuclei (CN) measurements at Cape Grim show that particle numbers do not increase markedly until the wind speed increases above 10 m/s (J. Gras, personal communication, 1999). In contrast δ_a increases from quite low wind speeds, possibly as result of the difference in the nature of the measurements. Wind generated aerosol may not make it to the *in situ* aerosol sampler at Cape Grim at low wind speed as a result of contact with the cliff. On the other hand, the measured δ_a result from the entire vertical atmospheric column, and so the impact of local topography will be less. Also, any variations in the vertical distribution of the sea-salt aerosol resulting from the changes in wind speed would affect δ_a, but not necessarily the near-ground *in situ* aerosol measurements.

Over the period of the δ_a record there have also been extensive measurements of *in situ* aerosol properties. It would be valuable to be able to correlate the two sets of measurements. However, this can be done only with additional information, as it is necessary to know the optical and physical properties of the aerosol throughout the aerosol layer. Firstly, this requires knowledge of the vertical extent of this boundary layer. This does not have a simple answer. LIDAR measurements show the presence of a boundary layer of around 400 to 600m in height with high laser backscatter, and then a second "buffer" layer extending up to 1900m with moderate backscatter [*Russell et al.*, 1998]. Secondly, the particle scattering is strongly dependent upon the relative humidity [*Carrico et al.*, 1998], especially at the 70-80% relative humidity experienced at Cape

Grim [*Jasper and Downey*, 1991]. It is also possible that the large numbers of particles generated by clouds just above the boundary layer may complicate matters, although they appear to contribute only a small fraction of the total extinction [*Clarke et al.*, 1998].

Within the limitations outlined above, the observed wind speed trends in δ_a can be compared to measurements of the wind speed dependence of aerosol mass concentration over oceans. The slope of the semi-log plot of δ_a versus wind speed (0.047 – 0.06) is less than the values in this region of 0.080 for large mode (centered around 0.3μm) winter aerosol [*Gras*, 1995], but similar to the 0.053 reported by Gras and Ayers [1983]. Values near 0.06 have also been found elsewhere [*Quinn et al.*, 1998]. Given the possible limitations of the comparison, there is a reasonable agreement between the determinations.

The absolute magnitude can also be roughly compared. If a sea-salt mass scattering efficiency of approximately 3 m^2 g^{-1} (for 30-45% RH, [*Quinn et al.*, 1998]) is doubled to allow for the impact of humidity, and a total salt mass of 10 μg m^{-3} is assumed (10m/s [*Gong et al.*, 1997]), the δ_a of 0.03 at this wind speed implies a boundary layer height of 500 m. Clearly the uncertainty in such an estimate is quite large, but it is in reasonable agreement with the LIDAR observations [*Russell et al.*, 1998].

Annual cycle without sea-salt

Using the observed wind-speed dependence, the data shown in Figure 5(a) can be corrected for the impact of sea-salt and the result of this is shown in Figure 5 (c). During the months April – June the residual δ_a is very small and not statistically significant. For the rest of the year, the overall annual pattern is largely unchanged. There is still a clear δ_a maximum in September, and a smaller maximum around February. Removing the estimated sea salt contribution, is equivalent to removing 40% of annual average δ_a.

Included in Figure 7(a) is the cycle in condensation nuclei, calculated as the average of the monthly median values for the period 1986 -1996 [See *Gras*, 1999, and previous issues]. It can be seen that the winter (June) minimum and the February maximum in the CN measurements is in broad agreement with features in the δ_a annual cycle. However, there is no corresponding September maximum in the *in situ* aerosol measurements.

Two other sources of the September peak in the aerosol optical depth can be discounted. There is a Winter/Spring maximum in stratospheric δ_S, but the stratospheric cycle is smaller than the cycle observed at Cape Grim, and has already been subtracted from the observations. Similarly, the upper tropospheric δ_a derived from SAGE II are too small [*Kent et al.*, 1998] to play a major role.

The size of the particles involved in the annual cycle of the residual δ_a can be broadly inferred from the ratio $R(\lambda_2,\lambda_1)=\delta_a(\lambda_2)/\delta_a(\lambda_1)$, a by-product of the general method analysis [*Forgan*, 1994]. Based on the Ångstrom formulation of the wavelength dependence this can be expressed as α, calculated using:

$$\alpha = -\frac{\log(\delta_{\lambda 2}/\delta_{\lambda 1})}{\log(\lambda_2/\lambda_1)}, \qquad (5)$$

where $\delta_{\lambda 1}$ is the aerosol optical depth at the wavelength λ_1. The α values based on $R(\lambda_2,\lambda_1)$ with λ_1 = 868nm are shown in Figure 7(b). The ratio determined using the general method is more stable than the ratios determined from equations (2) and (3), and less ambiguous than the results using δ_a. By their very nature $R(\lambda_2,\lambda_1)$ has been derived including stratospheric aerosol. To remove the stratospheric component requires the use of the optical depth at the reference wavelength (868nm in this case), and this introduces greater uncertainty. To overcome this a broader exclusion period (7/1991 – 6/1994) has been used. This results in a 20% reduction in total data, but the confidence intervals are half as large as that obtained from a stratospheric corrected data set.

The annual cycle of α clearly shows the size variations occurring in both February - March and September at 368nm. The data also suggests that while both periods involve an increase in small aerosol, there is a significant difference in the extinction behavior. The February maximum does not follow an Ăngstrom wavelength dependence, whereas the September peak does, within the scatter in the data.

All this points to quite different sources for the tropospheric aerosol observed during the year. The February maximum is likely to be due to the photochemical generation of aerosol within the marine boundary layer, as detected by the *in situ* CN counter, with the "non-Ắngstrom" behaviour indicating multiple aerosol populations.

The September peak is unlikely to be due to marine boundary layer aerosol. A likely source is mid-troposphere long-range transport. An analysis of gas samples collected at altitudes up to 8 km [*Pak et al.*, 1996] has shown that there is a maximum in CO in the region between 5 and 8km in September. They suggest that this is due to long-range transport of biomass burning products from regions in the southern tropics. It seems reasonable that aerosol will also be transported from such fires, and it could contribute to δ_a. A preliminary analysis of δ_a at 6 other sites in extra-tropical regions of Australia shows a similar spring maximum (data not presented here), suggesting that this is a broad scale phenomena, arguing against more local causes such as cloud production [*Clarke et al.*, 1998].

When all the dependencies described above (stratosphere, wind and annual cycle) are removed from the data there is evidence of structure remaining in the residual. This can be partially seen in Figure 4(b). The structure is related between the wavelengths indicative of aerosol extinction. However, with a standard deviation in the residual of only 0.01, it is not possible to conclusively interpret any such structure. Clearly such an analysis will require measurements made with an instrument with a significantly more stable calibration, and most likely at a more optically and equipment "friendly" location.

The data reported here are available as transmissions (S/S_0) from the Cape Grim Baseline Air Pollution Station or from the authors, upon request.

Conclusions

An analysis of 14 years of δ_a data at Cape Grim shows the influence of a number of different factors under clean air conditions. The Mt Pinatubo eruption in 1991 significantly altered δ_a for several years, with an apparently exponential decay of 19 ± 2 months. A brief second peak in 1997 is less well understood. Outside the period severely affected by Mt Pinatubo the optical depth is generally less than 0.05 at all wavelengths. In winter, when δ_a is at its lowest, there is a distinct wind dependence, indicating that the scattering at this time is primarily due to sea salt. A broad summer maximum is coincident with the *in situ* CN peak and is consistent with the impact of photochemically generated aerosol particles. A September maximum appears not to be related to marine aerosol, and it seems likely that this is caused by long-range transport of biomass burning products. This proposition is supported by vertical CO profiles and preliminary δ_a measurements made elsewhere in Australia.

Acknowledgements

This work was made possible by the financial support of the Cape Grim Baseline Air Pollution Station and the dedicated efforts of the staff at the station, for which we are very grateful.

References

Atkinson, R.J., and J.R. Easson, Revaluation of the Australian Total Column Ozone Data Record, in *Ozone in the Atmosphere*, edited by R.D. Bojkov, and P. Fabian, pp. 168, A. Deepak, Hampton, Va, 1989.

Beardsmore, D.J., and G.I. Pearman, Atmospheric carbon dioxide measurements in the Australian region: data from surface observatories, *Tellus*, *39B*, 42-66, 1987.

Beyerle, G., A. Herber, R. Neuber, and H. Gernandt, Temporal Development of Mt Pinatubo Aerosols As Observed By Lidar and Sun Photometer At Ny-Alesund, Spitsbergen, *Geophysical Research Letters*, *22* (18), 2497-2500, 1995.

Carrico, C.M., M.J. Rood, and J.A. Ogren, Aerosol Light Scattering Properties At Cape Grim, Tasmania, During the First Aerosol Characterization Experiment (Ace 1), *Journal of Geophysical Research-Atmospheres*, *103* (D13), 16565-16574, 1998.

Clarke, A.D., J.L. Varner, F. Eisele, R.L. Mauldin, D. Tanner, and M. Litchy, Particle Production in the Remote Marine Atmosphere - Cloud Outflow and Subsidence During ACE 1, *Journal of Geophysical Research-Atmospheres*, *103* (D13), 16397-16409, 1998.

Dick, A.L., S.R. Wilson, P.P. Took, and P.J. Fraser, Impact of regional sources on baseline measurements of nitrous oxide, in *Baseline Atmospheric Program (Australia) 1994-95*, edited by R.J. Francey, A.L. Dick, and N. Derek, pp. 30-40, Bureau of Meteorology in cooperation with CSIRO Division of Atmospheric Research, Melbourne, 1996.

Ethridge, D., G.R. Patterson, and C.M.R. Platt, Measurement of Aerosol Optical Depth (Turbidity) at Cape Grim 1978 - 1982, in *Baseline Atmospheric Program (Australia) 1981-82*, edited by R.J. Francey, pp. 51-54, Dept. of Science and Technology and CSIRO, Canberra, 1984.

Forgan, B.W., Determination of aerosol optical depth at a sea level station - investigations at Cape Grim BAPS, Cape Grim Baseline Air Pollution Station, 1987.

Forgan, B.W., Bias in a solar constant determination by the Langley method due to structured atmospheric aerosol: comment, *Applied Optics*, *27* (12), 2546-2548, 1988.

Forgan, B.W., General Method For Calibrating Sun Photometers, *Applied Optics*, *33* (21), 4841-4850, 1994.

Gong, S.L., L.A. Barrie, and J.-P. Blanchet, Modeling sea-salt aerosols in the atmosphere, 1, Model Development, *Journal of Geophysical Research*, *102*, 3805-3818, 1997.

Gras, J.L., Cn, Ccn and Particle Size In Southern Ocean Air At Cape Grim, *Atmospheric Research*, *35* (2-4), 233-251, 1995.

Gras, J.L., Particles, in *Baseline Atmospheric Program Australia 1996*, edited by J.L. Gras, N. Derek, N.W. Tindale, and A.L. Dick, pp. 126-129, Bureau of Meteorology and CSIRO Atmospheric Research, Melbourne, 1999.

Gras, J.L., and G.P. Ayers, Marine aerosol at southern mid-latitudes, *Journal of Geophysical Research*, *88* (C15), 10661-10666, 1983.

Herber, A., L.W. Thomason, K. Dethloff, P. Viterbo, V.F. Radionov, and U. Leiterer, Volcanic Perturbation of the Atmosphere in Both Polar Regions - 1991-1994, *Journal of Geophysical Research-Atmospheres*, *101* (D2), 3921-3928, 1996.

ISO, *Guide to the Expression of Uncertainty in Measurement*, International Organization for Standardization, Geneva, 1995.

Jasper, J.D., and A.H. Downey, Towards a Cape Grim Climatology, in *Baseline Atmospheric Program Australia 1989*, edited by S.R. Wilson, and J.L. Gras, pp. 38-46, Bureau of Meteorology and the CSIRO Division of Atmospheric Research, Melbourne, 1991.

Kent, G.S., C.R. Trepte, and P.L. Lucker, Long-Term Stratospheric Aerosol and Gas Experiment I and Ii Measurements of Upper Tropospheric Aerosol Extinction, *Journal of Geophysical Research-Atmospheres*, *103* (D22), 28863-28874, 1998.

Nagel, D., A. Herber, L.W. Thomason, and U. Leiterer, Vertical Distribution of the Spectral Aerosol Optical Depth in the Arctic From 1993 to 1996, *Journal of Geophysical Research-Atmospheres*, *103* (D2), 1857-1870, 1998.

Pak, B.C., R.L. Langenfelds, R.J. Francey, L.P. Steele, and I. Simmonds, A climatology of trace gases from the Cape Grim overflights, 1992-1995, *Baseline Atmospheric Program (Australia) 1994-1995*, 41-52, 1996.

Platt, C.M.R., and G.R. Patterson, The Interpretation of Baseline Atmospheric Turbidity Measurements at Cape Grim, Tasmania, *Journal of Atmospheric Chemistry*, *4*, 187-197, 1986.

Quinn, P.K., D.J. Coffman, V.N. Kapustin, T.S. Bates, and D.S. Covert, Aerosol Optical Properties in the Marine Boundary Layer During the First Aerosol Characterization Experiment (ACE 1) and the Underlying Chemical and Physical Aerosol Properties, *Journal of Geophysical Research-Atmospheres*, *103* (D13), 16547-16563, 1998.

Russell, L.M., D.H. Lenschow, K.K. Laursen, P.B. Krummel, S.T. Siems, A.R. Bandy, D.C. Thornton, and T.S. Bates, Bidirectional Mixing in an ACE 1 Marine Boundary Layer Overlain By a Second Turbulent Layer, *Journal of Geophysical Research-Atmospheres*, *103* (D13), 16411-16432, 1998.

Russell, P.B., J.M. Livingston, R.F. Pueschel, J.J. Bauman, J.B. Pollack, S.L. Brooks, P. Hamill, L.W. Thomason, L.L. Stowe, T. Deshler, E.G. Dutton, and R.W. Bergstrom, Global to Microscale Evolution of the Pinatubo Volcanic Aerosol Derived from Diverse Measurements and Analyses [Review], *Journal of Geophysical Research-Atmospheres*, *101* (D13), 18745-18763, 1996.

Sibson, B., and B.W. Forgan, CGBAPS active tracker system for equatorial mounts, in *Baseline Atmospheric Program (Australia) 1985*, edited by B.W. Forgan, and P.J. Fraser, pp. 38-41, Bureau of Meteorology in cooperation with CSIRO Division of Atmsopheric Research, Melbourne, 1987.

Thomason, L., SAGE II Stratospheric Aerosol Data Products, http://www-arb.larc.nasa.gov/sage2/data/aerosol/stratospheric/, 1998.

Walford, P., Introduction to the Cape Grim computer system (GRIMCO), in *Baseline Atmospheric Program (Australia) 1985*, edited by B.W. Forgan, and P.J. Fraser,

pp. 34-36, Bureau of Meteorology in cooperation with the CSIRO Division of Atmospheric Research, Melbourne, 1987.

WMO, Building instructions for WMO/PMOD sunphotometers, Geneva, 1979.

WMO, Report on the measurements of Atmospheric Turbidity in BAPMoN, 1994.

Woodcock, A.H., Salt nuclei in marine air as a function of altitude and wind force, *Journal of Meteorology*, *10*, 362-371, 1953.

Young, A.T., Observational technique and data reduction, in *Methods of Experimental Physics*, edited by N. Carleton, pp. 123-192, Academic Press, New York, 1974.

Figures

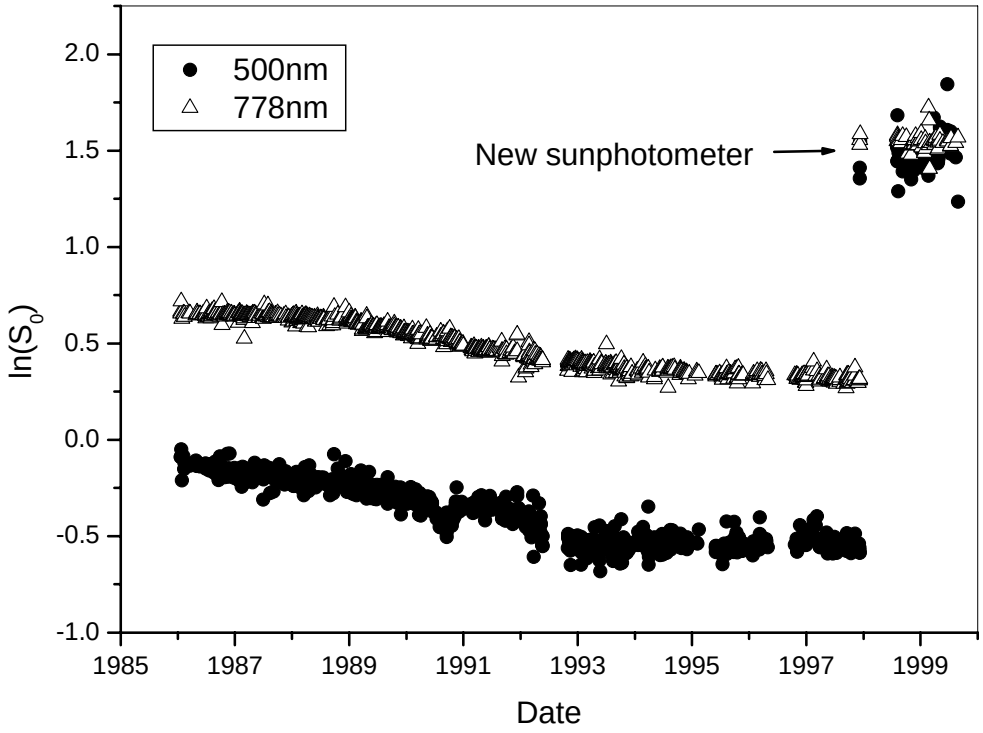

Figure 1

Figure 1 Calibration values for two wavelengths of the WMO#1 and SPO1A radiometers at Cape Grim.

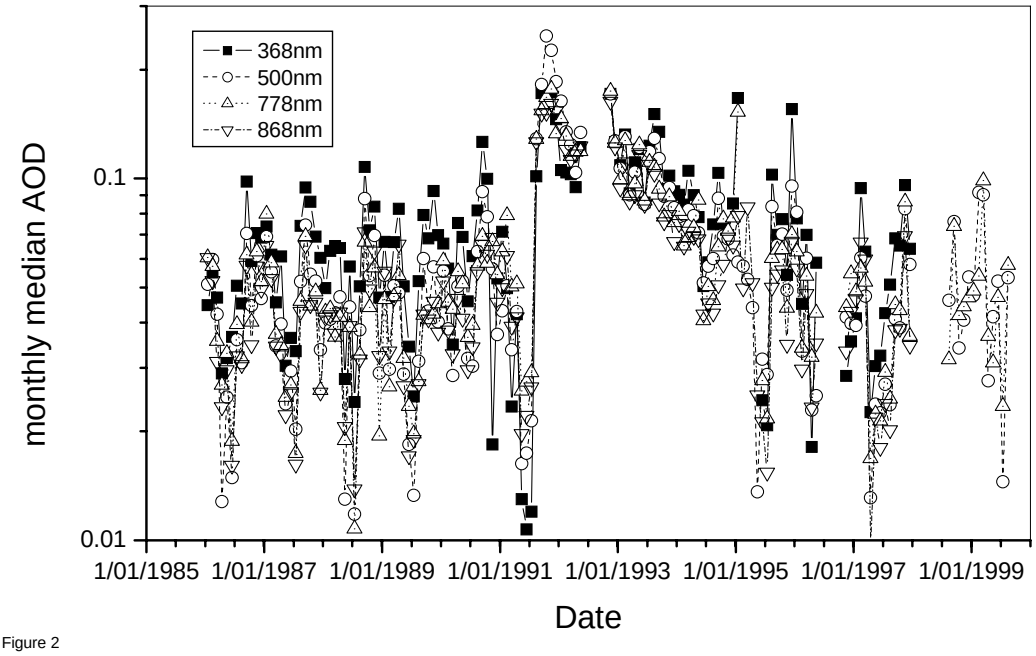

Figure 2

Figure 2: Monthly median aerosol optical depth ($\overline{\delta}_a$) at Cape Grim. See text for definitions. Values have not been filtered by wind direction. Monthly mean data have not been included if the month contains only one half-day of data.

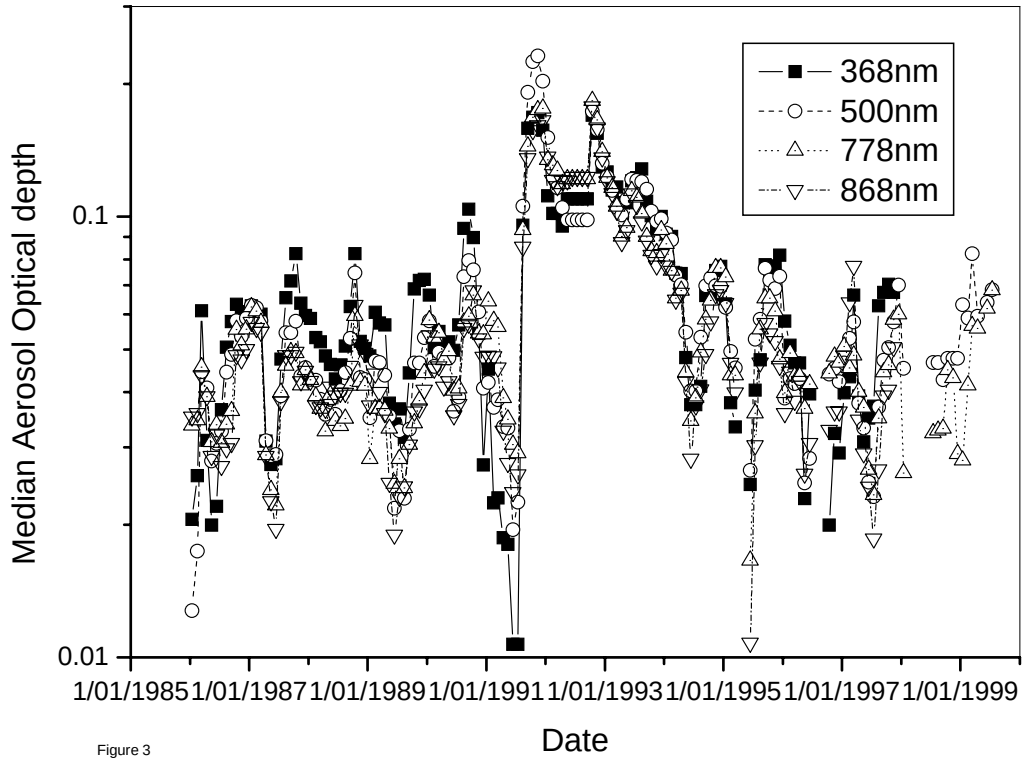

Figure 3: Median aerosol optical depth at Cape Grim, using $\overline{\delta}_a$ data selected as representative of the baseline wind sector (190 – 280°). The results have been calculated using a 90-day running median, centred on each month.

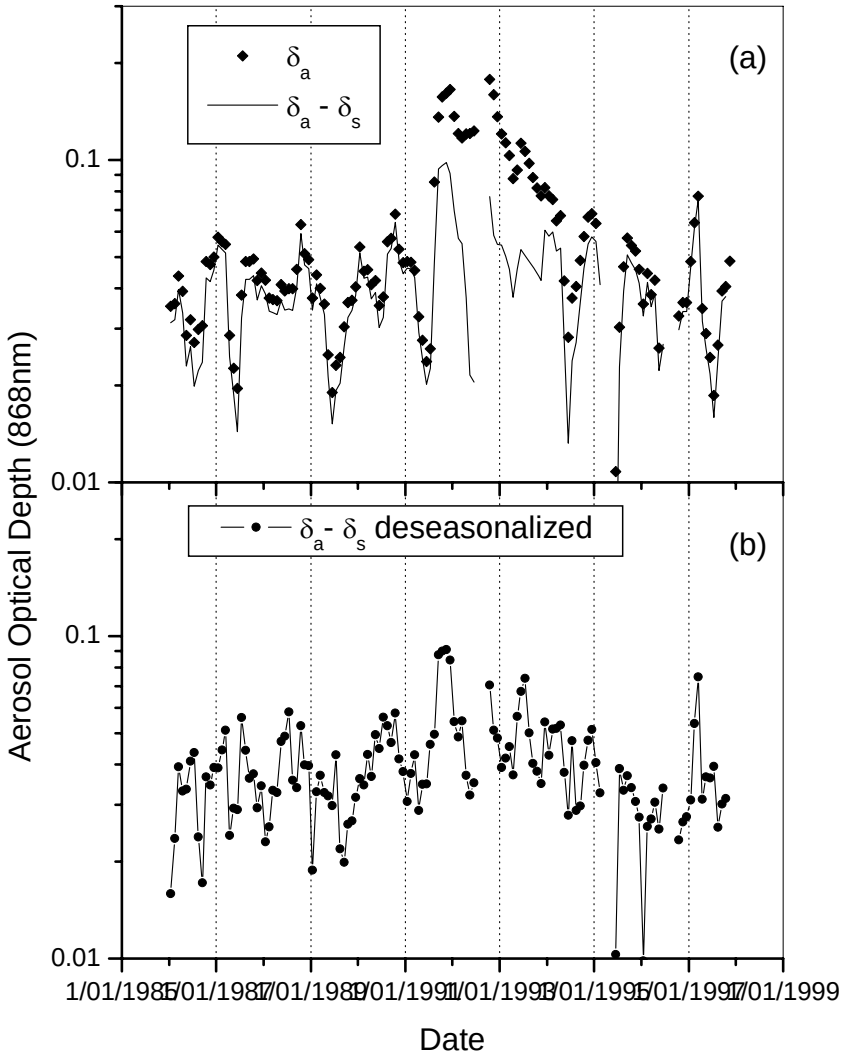

Figure 4

Figure 4: Monthly mean 868nm aerosol optical depths at Cape Grim under baseline conditions (wind from 190 - 280°). All results have been smoothed with a running 90-day average. Panel (a) shows the original data set (δ_a) and the results following removal of stratospheric aerosol based on SAGE II monthly average aerosol estimates ($\delta_a - \delta_s$). Panel (b) shows the time series of ($\delta_a - \delta_s$) deseasonalized, using the annual cycle of optical depth given in Table 1.

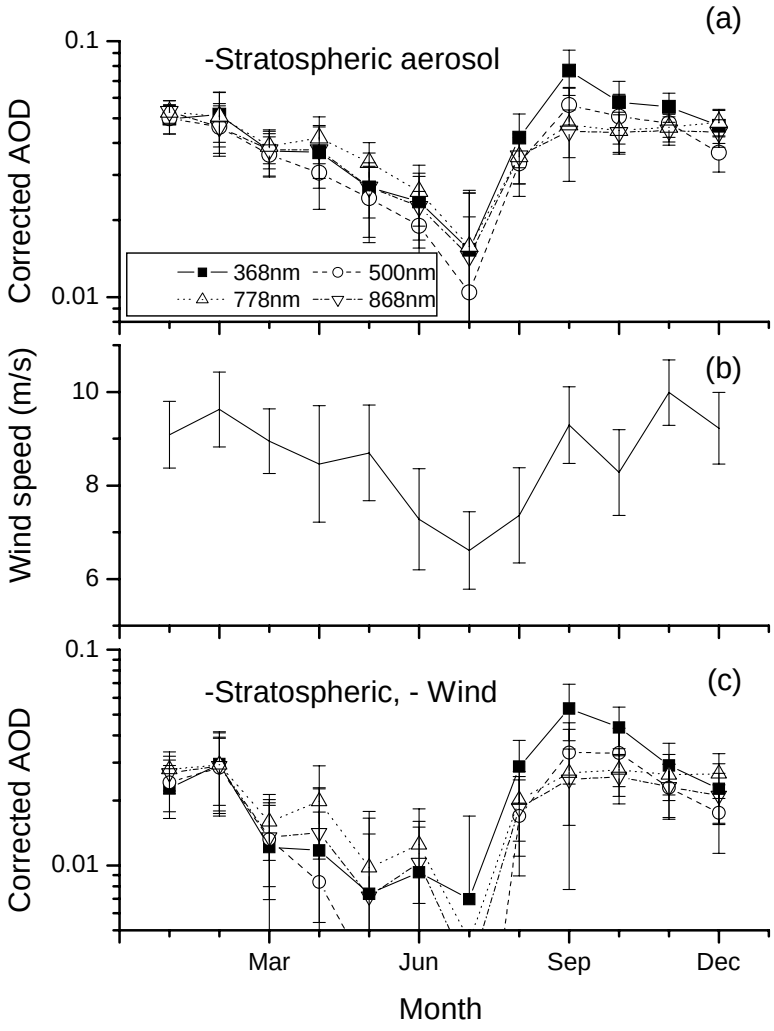

Figure 5

Figure 5: Median monthly aerosol optical depth at Cape Grim, with stratospheric aerosol removed. The error bars are the 95% confidence limits. In panel (a) the period 7/1991 – 6/ 1992 has been excluded from the analysis. Panel (b) shows the median wind speed calculated for the periods in which measurement was made. Panel (c) shows the annual cycle of aerosol optical depth as in panel (a), but with the wind dependent sea-salt component removed.

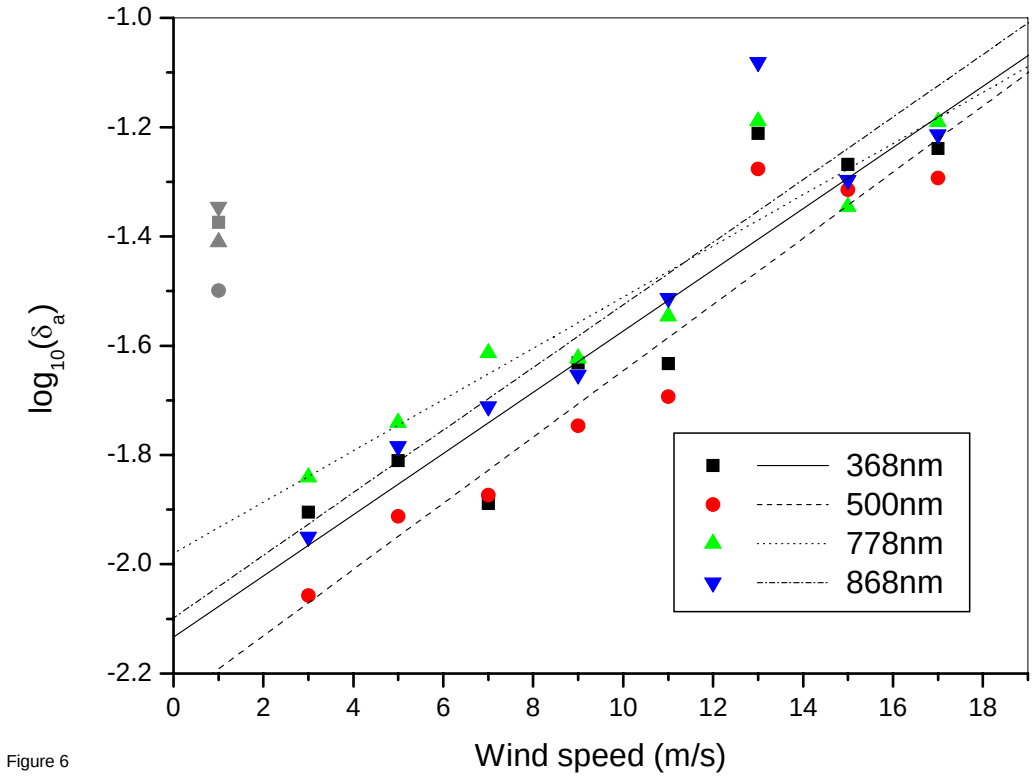

Figure 6

Figure 6: Aerosol optical depth in June and July as a function of wind speed. Stratospheric aerosol optical depth has been removed, and data selected for baseline periods. Data is shown for the period 1986–1997, excluding the period disturbed by Mt. Pinatubo. The linear regression fits shown excluding the wind speeds < 2 m/s.

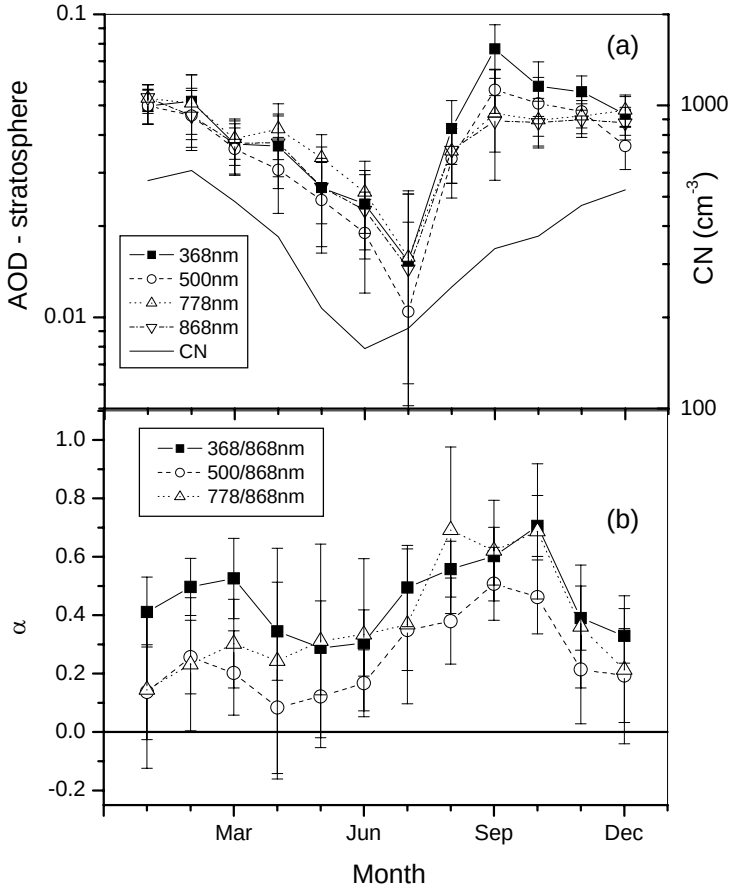

Figure 7

Figure 7: Annual cycle of aerosol optical depth determined for the period 1986 – 1997 inclusive. Error bars are 95% confidence limits. Panel (a) shows the aerosol optical depth excluding the SAGE II stratospheric component. The (6/1991 – 6/1992) data has been removed to remove the effect of the Mt. Pinatubo volcanic aerosol cloud. Also shown is the CN record for Cape Grim for the period 1986-1996. Panel (b) shows the values of the size parameter α as derived for the 3 wavelength ratios. This data includes the stratospheric component, as discussed in the text.

Table 1 Annual cycle of aerosol optical depth at four wavelengths for the period 1986 - 1999. The period affected by Mt. Pinatubo (6/1991 – 6/1992) and the stratospheric aerosol component has been removed, as described in the text. Figures in brackets are the 95% confidence limits. The annual average is calculated from the monthly means, to reduce the bias towards summer months where many more measurements are possible.

Month	368nm	500nm	778nm	868nm
1	0.050 (0.006)	0.050 (0.007)	0.053 (0.006)	0.053 (0.005)
2	0.052 (0.011)	0.046 (0.011)	0.051 (0.012)	0.046 (0.010)
3	0.037 (0.008)	0.036 (0.006)	0.039 (0.006)	0.038 (0.006)
4	0.037 (0.010)	0.031 (0.009)	0.042 (0.009)	0.038 (0.009)
5	0.027 (0.010)	0.024 (0.008)	0.034 (0.006)	0.027 (0.007)
6	0.024 (0.007)	0.019 (0.007)	0.026 (0.007)	0.023 (0.007)
7	0.015 (0.010)	0.010 (0.010)	0.016 (0.010)	0.014 (0.012)
8	0.042 (0.010)	0.033 (0.009)	0.035 (0.008)	0.036 (0.008)
9	0.077 (0.015)	0.056 (0.009)	0.047 (0.019)	0.044 (0.009)
10	0.058 (0.012)	0.051 (0.011)	0.045 (0.008)	0.044 (0.008)
11	0.055 (0.007)	0.048 (0.006)	0.046 (0.006)	0.045 (0.006)
12	0.047 (0.007)	0.037 (0.006)	0.048 (0.006)	0.044 (0.005)
Annual Average	0.043	0.037	0.040	0.038